

Estimating Radiative Properties in Porous Medium Using Micro-Scaled Additive Manufacturing and Machine Learning

Farhin Tabassum, Shima Hajimirza*

Department of Mechanical Engineering, Stevens Institute of Technology, Hoboken, USA - 07030

Abstract

In this study, we use an ultra-high-resolution micro-fabrication of porous media using two-photon polymerization (TPP) direct green laser writing maskless technology. By leveraging nonlinear light-matter interactions, using this process we can achieve sub-diffraction-limited features without the layer-by-layer constraints of traditional additive manufacturing. We print the structures using an inverted optical microscope with a 20X objective lens by tuning process parameters *i.e.*, refractive index of photoresist, laser power, printing speed, and exposure time to closely match the CAD design. After printing, we develop the samples using a chemical bath and assess their quality using scanning electron microscopy (SEM) images. We then measure their optical radiative properties using a micro-spectrophotometer across the 400nm - 750 nm range. To validate these results, we then compare them against Monte Carlo ray tracing (MCRT) simulations and Machine Learning (ML) predictions, observing a deviation of $\sim < 5\% - 8\%$. Overall, this study aims to establish an integrated framework where experimental results are validated through MCRT simulations and accelerated using ML-based predictions of radiative properties. This high-precision, low-waste fabrication approach offers consistent radiative properties with computational models and shows strong potential for engineering applications in micro-optics, photonics, solar energy, and metamaterials.

1. Introduction

The optical radiative properties of porous media are critical for their integration into energy-efficient devices[1–3]. Characterizing these properties has been extensively studied, with computational methods such as Monte Carlo ray tracing(MCRT)[4–8], renewal theory to derive explicit analytical estimates achieving close agreement with Monte Carlo Ray Tracing results[9] and finite-difference time-domain (FDTD) simulations[10,11] emerging as key approaches at the micro and nanoscale[12]. To mitigate the high computational costs associated with these methods[4,9], researchers have explored machine learning algorithms for predictive modeling of radiative properties[5,13–16]. However, the fabrication of energy-efficient devices remains challenging, especially as the structural scale of porous media approaches the micro- or nanoscale. Recent advancements in deposition techniques have shown promise, but micro- and nanoscale additive manufacturing[17–20] offers a more sophisticated and precise solution for fabricating stochastic porous media. Additive manufacturing has evolved from a prototyping tool into one of the widely adopted production methods in various engineering applications especially in industries[21–23]. This growth is driven by its capability in the production of complex geometries, material waste minimization, and rapid design iterations[24,25]. There are several types of additive manufacturing, one of which involves processes based on liquids, especially useful in micro- and nanofabrication

Liquid-based additive manufacturing[26] techniques, *e.g.*, stereolithography (SLA), digital light processing (DLP), and two-photon polymerization (2PP) work by curing photoresists with laser light exposure. These methods deliver unparalleled precision and high-resolution capabilities, making them well-suited for fabricating intricate micro-scaled structures. However, they are constrained by slower build times for larger structures, limited material options restricted to specific resins, and high operational costs. Despite these drawbacks, liquid-based methods are indispensable for applications

*Corresponding Author

E-mail address: shima.hajimirza@stevens.edu (S. Hajimirza)

requiring precise, high-resolution manufacturing. Among them, two-photon polymerization (TPP) [27,28] which allows for the fabrication of complex three-dimensional micro and nano-scaled structures with sub-diffraction-limit resolution as low as 100nm. TPP is a key component of sophisticated microscale production because of its versatility in working with a wide range of materials, such as metals, polymers, hybrid composites, and organically modified ceramics.

In this study, we present an additive manufacturing method for fabricating single-layered porous media using the TPP technique. The fabricated layers have thicknesses ranging from 1 μm to 5 μm , with random pore orientations and porosities of approximately 30% to 65%. The optical radiative properties such as absorptivity, transmissivity, reflectivity, and scattering are measured using a micro-spectrophotometer over the wavelength range of 400 nm to 750 nm. To assess the dimensional accuracy, and precision of fabrication, we perform Scanning Electron Microscopy (SEM) imaging analysis at a magnification of 700x and 1500x, operating at 5 kV voltage with a working distance of 10mm. These analyses provide detailed insights into potential distortions or dislocations in the fabricated porous structures. We then compare the precision of radiative property measurements with Monte Carlo ray tracing simulations. To reduce the computational expenses of MCRT, we train a customized machine learning (ML) model to predict radiative properties and compare the results with experimental measurements. This two-stage verification process reveals the possibility of fabricating true-scale microporous structures and evaluate their radiative behavior using both MCRT simulations and ML predictions with less than 5% deviation.

2. Experimental and Computational Methodology

In this section, we demonstrate the methodology in three different steps, Section 2.1 details the experimental procedure, Section 2.2, and 2.3 details computational procedures – Monte Carlo ray tracing (MCRT) and Machine Learning.

2.1 Fabrication of porous media

The fabrication and measurement procedures, based on the theoretical framework described in Section 2.1, are outlined in Figure 1. A Micro-light 3D micro-3D printer, a CRAIC Technologies

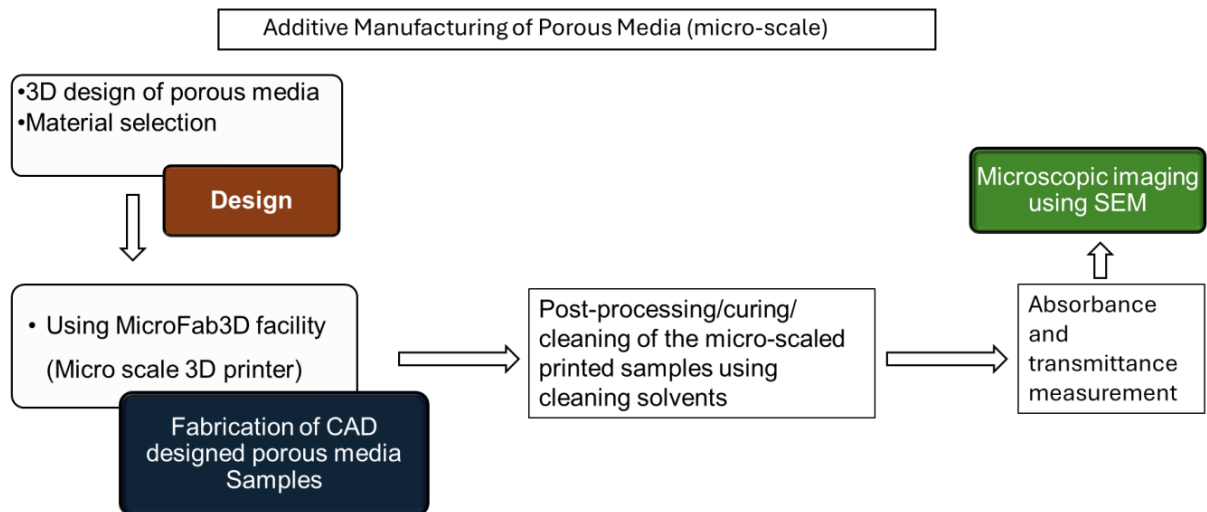


Figure 1. Process flow of the experimental procedure for additively manufactured micro-scaled porous medium.

micro- spectrophotometer, and a ThermoFisher Scientific (Apero 2) Scanning Electron Microscope (SEM) were employed for the experimental process. Fabrication is initiated by uploading a 3D CAD design of

porous medium in (.STL) format, ensuring precise replication of the porous medium. After optimizing the fabrication parameters, the porous structures were produced using the two-photon polymerization (TPP) technique, with pre-processing steps integrated into the Micro-light 3D system for sample preparation.

Figure 2 shows the images of the micro-3D printing setup by Micro-light 3D and the pre-processing step for sample fabrication. Figure 3 illustrates the 2D CAD design alongside optical microscope images of the fabricated samples at 20× and 40× magnifications, both pre-and post-processing. The CAD design is printed within the droplet of photoresist material deposited on a glass substrate

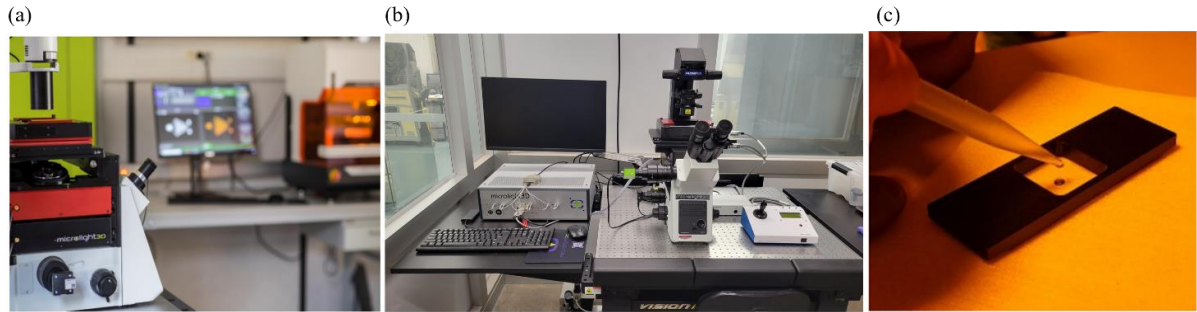


Figure 2. (a), (b) images of the 3D printing setup by Micro-light 3D, (c) sample preparation process

technique which follows non-linear two-photon absorption phenomenon and the technology is able to create a solid 3D-printed structure from a photoactivable material droplet of (thickness: ~0.17 mm; dimensions: 24 × 24 mm). The material underwent two-photon absorption in a highly localized volume, or "voxel," at the focal point, where a photopolymerization reaction solidified the liquid monomer into a polymeric structure. Using the above methodology, three monodisperse porous media samples were fabricated and subsequently characterized as shown in Figure 3.

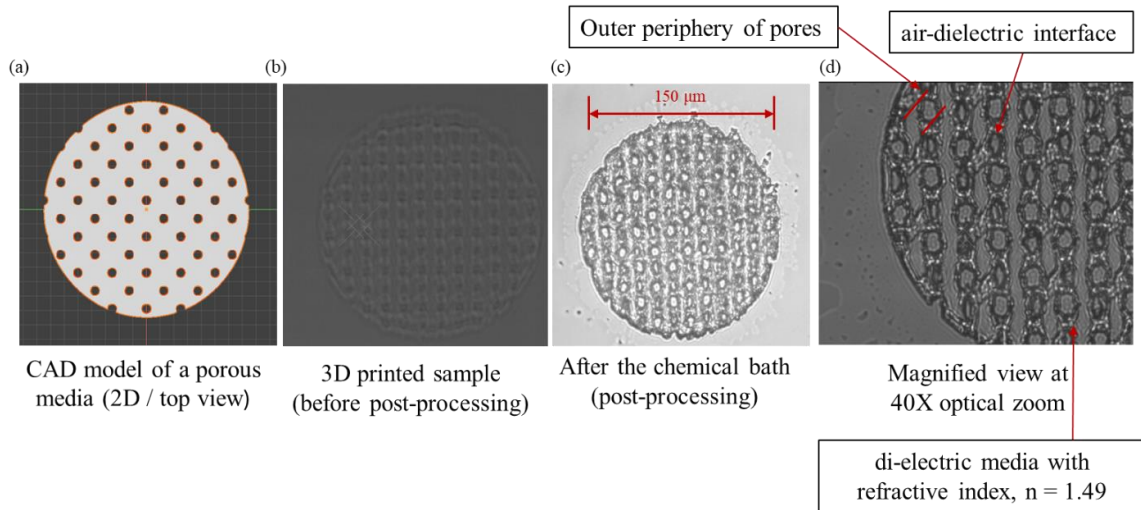


Figure 3. Steps followed in the 3D printer, (a) CAD model (.STL) file of the monodisperse porous structure with a diameter of 100μm, (b) printed sample under optical microscope before post-processing, (c) printed sample under optical microscope with 20X lens after post-processing (chemical bath), (d) printed sample at 40X magnification to demonstrate outer periphery of pores and air-dielectric interface.

2.2 Computational Methodology - Monte Carlo ray tracing (MCRT)

An energy bundle can be reflected, transmitted, and absorbed based on the following equation

$$\rho + \tau + \alpha = 1 \quad (1)$$

The reflectivity and transmissivity of an incident wave at the material discontinuity are computed using Fresnel's relation as follows assuming unpolarized light:

$$\rho = 0.5 \left(\frac{n_1 \cos \theta_2 - n_2 \cos \theta_1}{n_1 \cos \theta_2 + n_2 \cos \theta_1} \right)^2 + 0.5 \left(\frac{n_1 \cos \theta_1 - n_2 \cos \theta_2}{n_1 \cos \theta_1 + n_2 \cos \theta_2} \right)^2, \tau = 1 - \rho \quad (2)$$

The angle of refraction at the material discontinuity can be obtained based on Snell's law. The power attenuation of the ray is computed based on the traveling distance of the light through the absorbing medium which can be expressed according to Beer's law as follows:

$$E_f = E_i e^{-\beta s} \quad (3)$$

where E_i is the initial power of the light entering the domain is the extinction coefficient of the absorbing medium and shows the traveling distance of the light. The engineering features used in this study include mean and variance of the area, perimeter, convexity, bounding box, extent, solidity, and eccentricity of particles, mean horizontal and vertical lineal path distribution (forward and backward), two-point correlation function, averaged coordination number of particles, representative elementary volume, averaged coordination number of particles, chord length distribution, and tortuosity. The physics-based features include the porosity, refractive indices of the host and particle mediums, the initial angle of irradiation from the boundaries, and the coordinates of the emission.

2.3 Computational Methodology – Machine Learning (ML)

After ground truth (labeling) dataset generation, mentioned in Section 2.2, we apply a customized bounding box algorithm which creates imaginary bounding boxes around each pore to calculate the geometric features of the particles. We then proceed to extract in-vitro geometric features, *i.e.*, directional geometric metrics to define the position distribution. To do so, we use a machine learning (ML) model. For the final model, we employ a series of convolutional and pooling layers following Eqns. (4) – (7) below.

$$\zeta_{CNN} = Conv_{\theta_{CNN}}(X_{geom-image}) \quad (4)$$

$$\zeta_{CNN} = MaxPooling(\zeta_{CNN}) \quad (5)$$

$$\zeta_{CNN} = Conv_{\theta_{CNN}}(\zeta_{CNN}) \quad (6)$$

$$\zeta_{CNN} = MaxPooling(\zeta_{CNN}) \quad (7)$$

where θ_{CNN} represents learnable parameters, ζ_{CNN} represents feature map after the above operations and *MaxPooling* is the max-pooling operation. Simultaneously we have the tabular matrix of features extracted through bounding box algorithm as well as the input physical features for simulation. We combine them using the Eqn. (8) to concatenate extracted in-vitro directional features with their corresponding features in the tabular matrix.

$$\zeta_{hybrid} = Concatenate(\zeta_{CNN}, X_{features}) \quad (8)$$

Afterwards, we perform a deep learning operation on the combined datasets of ground truth and extracted features, to train and predict our desired radiative properties. The output layer ($l = L + 1$) which produces the network's prediction can be written using Eqns. (9) and (10) below:

$$\zeta^{(L+1)} = a^L * W^{(L+1)} + b^{(L+1)} \quad (9)$$

$$\hat{y}_i = \sigma^{(L+1)} (\zeta^{(L+1)}) \quad (10)$$

where, \hat{y}_i denotes the predicted outputs from ML model, L denotes the layers and σ is the activation function.

3. Results and Discussions

3.1 Radiative property measurement

The samples' optical radiative properties are measured using a micro-spectrophotometer (CRAIC Technologies) over the wavelength range of 400 nm to 750 nm for unpolarized light specified in Figure 4. The device employs a pixel-based approach to measure the absorptance of the surface area covered by each pixel. A pixel size of $50 \mu\text{m} \times 50 \mu\text{m}$ is selected to maximize sample coverage. During measurement, light is emitted from top to bottom along the Z-axis. The shadowed pixel enables the system to detect the overall absorptance within the defined volume.

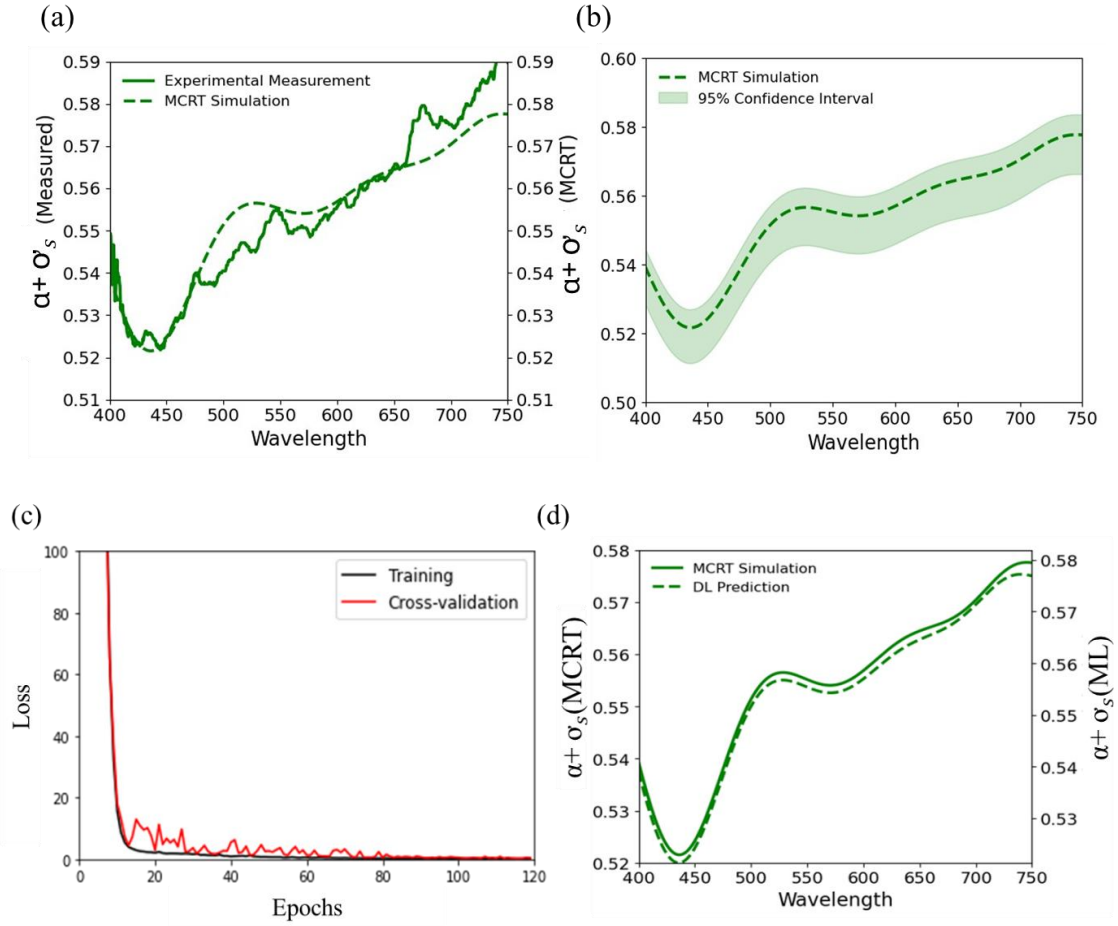


Figure 4. (a) Comparison between the measured absorptivity and scattering of the sample and the MCRT simulations, (b) 95% confidence interval of the MCRT simulations of the sample showing the measurable uncertainties from experimental results, (c) Training and cross-validation of ML model based on MCRT simulations, (d) comparison of MCRT simulations and ML model predictions to evaluate prediction accuracy

Figure 4 (a) shows experimentally measured absorptivity. From 400 nm to 450 nm, absorptivity decreases, but it begins to rise beyond 450 nm. This behavior is consistent with the inverse relationship

between absorptivity and scattering in porous media, where increased scattering typically results in lower absorptivity. In the media, scattering is wavelength-dependent, redistributing photon paths. However, the expected inverse relationship between absorptivity and scattering is disrupted between 450 nm and 700 nm. This deviation is likely attributable to the material's intrinsic properties, including its band gap energy, as well as scattering-induced light trapping, which effectively increases the optical path length of photons within the sample. Furthermore, the AM 1.5 solar irradiance spectrum exhibits a high photon flux in this range, which enhances light-matter interactions, thereby increasing absorptivity. Beyond 700 nm, as the photon flux diminishes in the AM 1.5 spectrum, the absorptivity trend realigns with the expected inverse relationship to scattering. This behavior underscores the role of porous structures in redirecting photons into absorbing regions, which boosts absorptivity and temporarily disrupts the typical inverse correlation between absorptivity and scattering. Figure 4(a) also shows the deviation between experimentally measured absorptivity and MCRT simulation obtained absorptivity. Figure 4(b) shows the deviation between MCRT simulations and ML predictions across the wavelength. Figure 4(c) shows an image defining the axis used to measure the optical radiative properties along the Z-axis. Figure 4(d) presents a comparison between the measured absorptance, and computational data obtained using Monte Carlo ray tracing. It also provides absolute error and mean absolute error between the two across the considered wavelength range.

3.2 Scanning Electron Microscopic (SEM) Imaging

For advanced characterization and high-resolution imaging of our additively manufactured mono-layered porous medium, we utilized a ThermoFisher Scientific Apero 2 Scanning Electron Microscope (SEM). Since the photoresist material used for fabrication is non-conductive, the surface was first coated with a few nanometers of gold sputtering to enhance conductivity. SEM imaging was then performed to analyze the fabricated sample. Figure 5(a) presents the SEM image of the sample at a 1 nm resolution, 700× magnification, 5 kV working voltage, and a 10 mm analytical working distance.

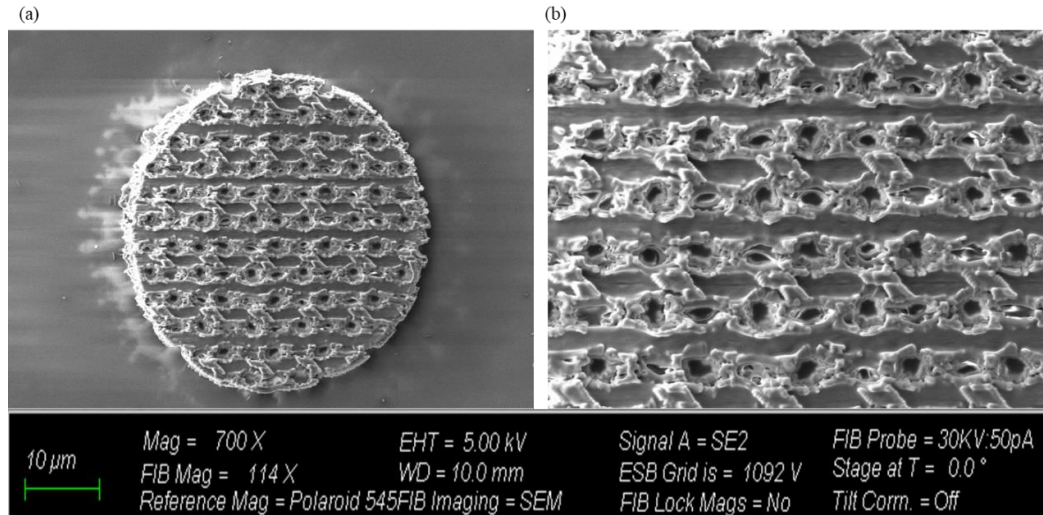


Figure 5. Scanning Electron Microscopy (SEM) images of the porous media sample, (a)700X magnification, (b) 1500X magnification.

Figure 5(b) provides a higher magnification (1500×) image highlighting the outer periphery of the pores and the metal-dielectric interface. This detailed imaging analysis allows for the refinement of fabrication parameters for micro-scaled additive manufacturing and facilitates comparison with computationally and analytically derived radiation loss values, offering insights for further optimization.

4. Conclusion

This paper presents a procedure for fabricating micro-scaled porous media via two-photon polymerization (TPP) and characterizing their optical radiative properties using a micro-spectrophotometer across the 400 nm to 750 nm wavelength range. Scanning Electron Microscopy (SEM) was employed for high-resolution imaging and materials analysis, providing critical data for optimizing the fabrication process and comparing radiation loss with computational and analytical models. This methodology enables the evaluation of the feasibility of fabricating complex porous media designs, previously studied computationally, and offers the potential for inverse design to fine-tune printing parameters. It also shows the possibility of integrating ML models to optimize the process of manufacturing energy-efficient optical devices, including thin-film solar cells and micro-phonic sensors.

5. Acknowledgement

Funding: The authors appreciate support by the United States National Science Foundation (NSF) under grant CBET- 2339032.

6. References

- [1] W. Fuqiang, Z. Xinping, D. Yan, Y. Hongliang, X. Shi, L. Yang, C. Ziming, Progress in radiative transfer in porous medium: A review from macro scale to pore scale with experimental test, *Applied Thermal Engineering* 210 (2022) 118331. <https://doi.org/10.1016/j.applthermaleng.2022.118331>.
- [2] C. Chen, C. Yang, D. Ranjan, P.G. Loutzenhiser, Z.M. Zhang, Spectral Radiative Properties of Ceramic Particles for Concentrated Solar Thermal Energy Storage Applications, *Int J Thermophys* 41 (2020) 152. <https://doi.org/10.1007/s10765-020-02733-5>.
- [3] S. Baghaei Oskouei, G.F. Frate, R. Christodoulaki, Ö. Bayer, İ.S. Akmandor, U. Desideri, L. Ferrari, V. Drosou, İ. Tari, Solar-powered hybrid energy storage system with phase change materials, *Energy Conversion and Management* 302 (2024) 118117. <https://doi.org/10.1016/j.enconman.2024.118117>.
- [4] F. Tabassum, A. Eghtesad, S. Hajimirza, Predicting light-matter interaction in semi-transparent elliptical packed beds using hybrid deep learning (HDL) approach, *Results in Engineering* 19 (2023) 101368. <https://doi.org/10.1016/j.rineng.2023.101368>.
- [5] F. Tabassum, S. Hajimirza, Enhancing Computational Efficiency in Porous Media Analysis: Integrating Machine Learning With Monte Carlo Ray Tracing, *Journal of Thermal Science and Engineering Applications* 16 (2024). <https://doi.org/10.1115/1.4065895>.
- [6] C. Chen, D. Ranjan, P.G. Loutzenhiser, Z.M. Zhang, A numerical study of the spectral radiative properties of packed bed with mixed bauxite and silica spheres, *International Journal of Heat and Mass Transfer* 207 (2023) 124025. <https://doi.org/10.1016/j.ijheatmasstransfer.2023.124025>.
- [7] K. Lin, M. Pourmajidian, F.K. Suleiman, J.R. McDermid, K.J. Daun, Interpreting the radiative properties of advanced high strength steel strip using a hybrid thin film/geometric optics model, *Journal of Quantitative Spectroscopy and Radiative Transfer* 277 (2022) 107963. <https://doi.org/10.1016/j.jqsrt.2021.107963>.
- [8] R. Eze, A. Rahman, S. Kumar, Modeling Energy Deposition in Very Thin Layered Media by Monte Carlo Simulation, in: n.d. <https://doi.org/10.1115/BioMed2007-38042>.
- [9] S. Hajimirza, Precise derivations of radiative properties of porous media using renewal theory, *Journal of Quantitative Spectroscopy and Radiative Transfer* 310 (2023) 108709. <https://doi.org/10.1016/j.jqsrt.2023.108709>.
- [10] F. Tabassum, G.-R. Domenikos, S. Hajimirza, Using Hybrid Deep Learning to Predict Spectral Responses of Quantum Dot-Embedded Nanoporous Thin-Film Solar Cells, *Journal of Quantitative Spectroscopy and Radiative Transfer* (2024) 109258. <https://doi.org/10.1016/j.jqsrt.2024.109258>.

- [11] M. Kaya, S. Hajimirza, Extremely Efficient Design of Organic Thin Film Solar Cells via Learning-Based Optimization, *Energies* 10 (2017) 1981. <https://doi.org/10.3390/en10121981>.
- [12] S. Shan, C. Chen, P.G. Loutzenhiser, D. Ranjan, Z. Zhou, Z.M. Zhang, Spectral emittance measurements of micro/nanostructures in energy conversion: a review, *Front. Energy* 14 (2020) 482–509. <https://doi.org/10.1007/s11708-020-0693-0>.
- [13] S. Hajimirza, H. Sharadga, Learning thermal radiative properties of porous media from engineered geometric features, *International Journal of Heat and Mass Transfer* 179 (2021) 121668. <https://doi.org/10.1016/j.ijheatmasstransfer.2021.121668>.
- [14] F. Tabassum, A. Egthesad, G.-R. Domenikos, S. Hajimirza, ESTIMATING RADIATIVE PROPERTIES IN ARBITRARY POROUS MEDIA USING CASE-SPECIFIC DATA − DRIVEN MACHINE LEARNING FRAMEWORKS, in: Begel House Inc., 2023. <https://www.dl.begelhouse.com/references/1bb331655c289a0a,6aab6e2d4fa83503,0b6465270be92801.html> (accessed August 10, 2023).
- [15] N.S. Narayanan, F.K. Suleiman, W.M. Prada, M. Zuijderwijk, K.J. Daun, Artificial neural network for inferring radiative property variations across advanced high strength steel coils, *Journal of Quantitative Spectroscopy and Radiative Transfer* 318 (2024) 108928. <https://doi.org/10.1016/j.jqsrt.2024.108928>.
- [16] T. Akba, D.K. Baker, M.P. Mengüç, Geometric design of micro scale volumetric receiver using system-level inputs: An application of surrogate-based approach, *Solar Energy* 262 (2023) 111811. <https://doi.org/10.1016/j.solener.2023.111811>.
- [17] Z. Chen, Y.-T. Lin, H. Salehi, Z. Che, Y. Zhu, J. Ding, B. Sheng, R. Zhu, P. Jiao, Advanced Fabrication of Mechanical Metamaterials Based on Micro/Nanoscale Technology, *Advanced Engineering Materials* 25 (2023) 2300750. <https://doi.org/10.1002/adem.202300750>.
- [18] W. Lin, D. Chen, S.-C. Chen, Emerging micro-additive manufacturing technologies enabled by novel optical methods, *Photon. Res.*, PRJ 8 (2020) 1827–1842. <https://doi.org/10.1364/PRJ.404334>.
- [19] D. Behera, S. Chizari, L.A. Shaw, M. Porter, R. Hensleigh, Z. Xu, X. Zheng, L.G. Connolly, N.K. Roy, R.M. Panas, S.K. Saha, X. (Rayne) Zheng, J.B. Hopkins, S.-C. Chen, M.A. Cullinan, Current challenges and potential directions towards precision microscale additive manufacturing – Part IV: Future perspectives, *Precision Engineering* 68 (2021) 197–205. <https://doi.org/10.1016/j.precisioneng.2020.12.014>.
- [20] H.S. Khare, N.N. Gosvami, I. Lahouij, Z.B. Milne, J.B. McClimon, R.W. Carpick, Nanotribological Printing: A Nanoscale Additive Manufacturing Method, *Nano Lett.* 18 (2018) 6756–6763. <https://doi.org/10.1021/acs.nanolett.8b02505>.
- [21] G. Rasiya, A. Shukla, K. Saran, Additive Manufacturing-A Review, *Materials Today: Proceedings* 47 (2021) 6896–6901. <https://doi.org/10.1016/j.matpr.2021.05.181>.
- [22] O. Abdulhameed, A. Al-Ahmari, W. Ameen, S.H. Mian, Additive manufacturing: Challenges, trends, and applications, *Advances in Mechanical Engineering* 11 (2019) 1687814018822880. <https://doi.org/10.1177/1687814018822880>.
- [23] U.M. Dilberoglu, B. Gharehpapagh, U. Yaman, M. Dolen, The Role of Additive Manufacturing in the Era of Industry 4.0, *Procedia Manufacturing* 11 (2017) 545–554. <https://doi.org/10.1016/j.promfg.2017.07.148>.
- [24] B. Vayre, F. Vignat, F. Villeneuve, Designing for Additive Manufacturing, *Procedia CIRP* 3 (2012) 632–637. <https://doi.org/10.1016/j.procir.2012.07.108>.
- [25] S. Yang, Y.F. Zhao, Additive manufacturing-enabled design theory and methodology: a critical review, *Int J Adv Manuf Technol* 80 (2015) 327–342. <https://doi.org/10.1007/s00170-015-6994-5>.
- [26] F. Wang, F. Wang, Liquid Resins-Based Additive Manufacturing, *J. Mol. Eng. Mater.* 05 (2017) 1740004. <https://doi.org/10.1142/S2251237317400044>.
- [27] X. Zhou, Y. Hou, J. Lin, A review on the processing accuracy of two-photon polymerization, *AIP Advances* 5 (2015) 030701. <https://doi.org/10.1063/1.4916886>.
- [28] K.-S. Lee, D.-Y. Yang, S.H. Park, R.H. Kim, Recent developments in the use of two-photon polymerization in precise 2D and 3D microfabrications, *Polymers for Advanced Technologies* 17 (2006) 72–82. <https://doi.org/10.1002/pat.664>.